Ultrafast Time-Division Demultiplexing of Polarization-Entangled Photons

John M. Donohue,[1,*] Jonathan Lavoie,[1,2] and Kevin J. Resch[1]
[1]Institute for Quantum Computing and Department of Physics & Astronomy, University of Waterloo, Waterloo, Canada N2L 3G1
[2]Group of Applied Physics, University of Geneva, CH-1211 Genève 4, Switzerland
(Received 13 August 2014; published 16 October 2014)

Maximizing the information transmission rate through quantum channels is essential for practical implementation of quantum communication. Time-division multiplexing is an approach for which the ultimate rate requires the ability to manipulate and detect single photons on ultrafast time scales while preserving their quantum correlations. Here we demonstrate the demultiplexing of a train of pulsed single photons using time-to-frequency conversion while preserving their polarization entanglement with a partner photon. Our technique converts a pulse train with 2.69 ps spacing to a frequency comb with 307 GHz spacing which may be resolved using diffraction techniques. Our work enables ultrafast multiplexing of quantum information with commercially available single-photon detectors.

DOI: 10.1103/PhysRevLett.113.163602 PACS numbers: 42.50.Dv, 03.67.Hk, 42.65.Ky, 42.65.Re

Quantum communication promises unconditionally secure information transmission by exploiting fundamental features of quantum mechanics [1]. For many protocols, transmission channels capable of distributing entanglement between distant parties are required [2–4]. Furthermore, to be practical, these protocols must allow communication at high rates. One strategy which has successfully increased transmission rates in classical telecommunication is multiplexing, where ancillary degrees of freedom are utilized to carry independent modes copropagating through a single physical link, such as an optical fiber [5,6]. Some of these techniques have been adapted to quantum scenarios [7–13] and lay the groundwork for future quantum communication networks.

Time-division multiplexing [6] uses the arrival time of light pulses relative to an external clock to distinguish multiple communication modes. It is compatible with fiber-optic systems and is robust against birefringent effects. The delay between subsequent pulses must be greater than the timing jitter of the detection system to avoid cross talk between signals; for high rates, the delay must also be greater than detector dead time to detect photons from subsequent pulses. State-of-the-art single photon counting detectors have demonstrated 30 ps timing jitter and nanosecond-scale dead times [14]. However, it is possible in principle to distinguish between two pulses as long as they are separated by their coherence time, which can be orders of magnitude smaller in ultrafast applications. Single-photon measurement techniques for these time scales are therefore critical to optimize the quantum information capacity.

Techniques incorporating short laser pulses and nonlinear optical effects are key to manipulating light on ultrafast time scales [15–18]. In the quantum regime, such methods have enabled single- and entangled-photon frequency conversion [19–23], all-optical routing of quantum information [24,25], and ultrafast coincidence measurement for biphotons [26–28]. Additionally, ultrafast pulse shaping provides a diverse set of tools to tailor nonlinear optical interactions for customizing quantum optical waveforms [29–33], having found application in realizing coherent time-bin measurements on the picosecond time scale [34].

Drawing from these techniques, here we show a method for demultiplexing a rapidly pulsed sequence of polarization-encoded quantum states [Fig. 1(a)]. Any attempt to directly measure the polarization state of an individual pulse with a photon counter will be subject to cross talk from the other pulses due to the limited detector time resolution appearing as an incoherent mixture of the different states. We employ polarization-maintaining sum-frequency generation (SFG) with chirped pulses as a time-to-frequency converter to map ultrafast-scale time delays to measurable frequency shifts, thus allowing the individual quantum states to be read out using conventional diffraction techniques and photon detectors. Furthermore, our method manipulates the time-frequency characteristics of polarization-entangled photons, compressing their spectral bandwidth while preserving entanglement.

Our approach is based on sum-frequency generation between a chirped single photon and an oppositely chirped (antichirped) escort laser pulse. The spectrum of the SFG signal for strongly chirped pulses is much narrower than that of the input light and the frequency produced is linearly dependent on the relative delay between the pulses [32,35–37]. We quantify the dispersion applied using the chirp parameter A, defined as $A = \frac{1}{2}(d^2\phi/d\omega^2)$, where $\phi(\omega)$ is the spectral phase. If the chirps applied are equal and opposite, then the rms spectral bandwidth of the SFG signal is $\sigma_{\mathrm{SFG}} \leq 1/(2\sqrt{2}A\sigma)$, where σ is the smaller of the input bandwidths, and the frequency shift is $\Delta\omega = \tau/(2A)$ away from the sum of the input centre frequencies.

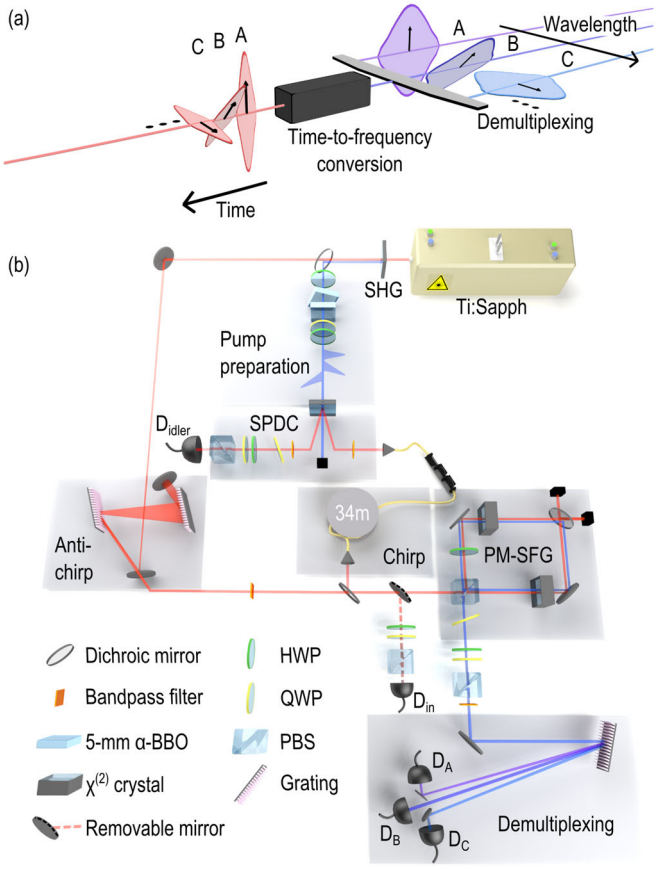

FIG. 1 (color online). Time-to-frequency conversion concept and experimental setup. (a) A train of temporally narrow polarized photonic signals A–C are converted into a comb of spectrally narrow and correspondingly polarized photons with a central frequency dependent on their time of arrival. The different frequency modes may then be demultiplexed using diffraction techniques. (b) Two α-BBO crystals and a series of wave plates prepared a train of pump pulses 2.69 ps apart, which were then used to create a pulse sequence of polarization-entangled states through SPDC. The single photons were chirped in single-mode fiber and combined with an antichirped strong escort pulse using a dichroic mirror. This beam was then focused in two 10-mm BiBO crystals arranged in a Sagnac configuration for polarization-maintaining sum-frequency generation (PM-SFG). The polarizations of the output photons were measured, and the three signals were then separated with a diffraction grating and coupled to detectors D_{A-C}. A removable mirror to D_{in} enabled measurement of the input state.

Through this mechanism, chirped-pulse up-conversion maps a train of temporally separated pulses into a comb of distinct frequencies.

We require that entanglement is preserved through this time-to-frequency conversion process. Because of phase-matching considerations, sum-frequency generation in nonlinear crystals is typically efficient for only a specific set of input polarizations, effectively measuring the polarization and destroying coherence. Preservation of the polarization, and hence the entanglement, can be achieved by coherently combining the output of two sum-frequency processes [23]. A full theoretical description of chirped-pulse up-conversion applied to a train of polarization-entangled states can be found in the Supplemental Material [38].

We create photon pairs using spontaneous parametric down-conversion [SPDC, Fig. 1(b)]. The pump is produced through second-harmonic generation (SHG) of an 80 MHz titanium-sapphire (Ti:sapph) femtosecond laser and has a center wavelength of 394.7 nm with a 1.45 nm full width at half maximum bandwidth (FWHM). Down-conversion is produced in a pair of orthogonally oriented 1-mm β-barium borate (BBO) crystals cut for type-I down-conversion [39,40]. The source converts pump photons in the polarization state $\alpha|H\rangle + \beta|V\rangle$ into down-converted pairs in the polarization state $\beta|HH\rangle + \alpha|VV\rangle$, where α and β are complex numbers; this can be a separable or entangled state depending on the polarization of the pump.

To create a dense train of pulsed photon pairs, we pass the pump through a series of rotatable birefringent crystals [pump preparation, Fig. 1(b)]. As the pump propagates through each crystal, the component polarized along the fast axis will lead the one polarized along the slow axis. If the temporal walk-off between these components is greater than the coherence time of the pump, the pump will exit as two pulses which are distinguishable in arrival time relative to a reference from the ultrafast laser source. Using n crystals of identical birefringence, a train of $n+1$ pulses may be created; if the crystal lengths differ, it is possible to create up to 2^n pulses [41]. This prepared pump creates a train of pulsed down-conversion, where the polarization state of each pair is determined by the polarization of the corresponding pump pulse. To create up to three temporally distinct down-conversion signals, labeled A–C from earliest to latest, we use two 5-mm α-BBO crystals cut for maximum birefringence; each apply a relative time delay of (2.69 ± 0.17) ps between orthogonal polarization modes. A complete description of the pump preparation setup and down-conversion scheme may be found in the Supplemental Material [38].

The signal photons pass through an interference filter centered at 809.06 nm with a 3.9 nm (or 1.8 THz) bandwidth (FWHM) before coupling into 34 m of single-mode fiber, applying positive dispersion corresponding to a chirp parameter of $A = (696 \pm 3) \times 10^3$ fs^2. Using a grating-based compressor [42], matched negative dispersion is applied to a 225 mW escort pulse at 786.2 nm with a 6.3 nm bandwidth (FWHM). The signal photons and escort pulse are then combined into a single beam with a dichroic mirror.

In order to implement polarization-maintaining SFG, we use a Sagnac-type interferometer [PM-SFG, Fig. 1(b)]. In this configuration, the horizontally and vertically polarized components of the signal photon are split on a polarizing beam splitter (PBS) and the vertical component

is rotated to horizontal polarization using an achromatic half-wave plate. Each beam is then upconverted independently in 10 mm of bismuth borate (BiBO) cut at 150.9° for type-I SFG. The SFG signal continues inside the Sagnac loop while the remaining escort is removed using a dichroic mirror. The horizontal component is flipped on the same achromatic half-wave plate and the two components are coherently recombined on the input PBS. A tilted quarter-wave plate sets the phase of the up-converted signal, ensuring that coherent superpositions of $|H\rangle$ and $|V\rangle$ are also maintained. The internal SFG efficiency was estimated to be 0.3%. The Sagnac geometry enables passive phase stability, preserving the input polarization state through the sum-frequency process over the 32-h runtime of the experiment.

After polarization measurement, the remaining near-infrared and escort second harmonic were removed with a bandpass filter. The signals were then separated with a 3600-lines/mm diffraction grating in near-Littrow configuration and allowed to propagate for 4.3 m in free space before being coupled via multimode fiber into three separate detectors, D_{A-C}. The combined diffraction and coupling efficiency was measured to be approximately 13%. The measured single-photon spectra were found to have an average bandwidth of (0.047 ± 0.007) nm, or, equivalently, (88 ± 13) GHz (Fig. 2). The spectra measured in modes A–C had respective central wavelengths of 398.936, 399.099, and 399.262 nm. This clearly shows that the three down-conversion pulses, 2.69 ps apart, were mapped to three distinct wavelengths separated by (0.163 ± 0.007) nm, or, equivalently, 307 GHz. This spacing is on the same order of magnitude as telecommunication standards for dense wavelength-division multiplexing [43].

To characterize the preservation of entanglement through our setup, we first prepared the pump to produce the maximally entangled state $|\Phi^+\rangle = (1/\sqrt{2})(|HH\rangle + |VV\rangle)$ in a *single* temporal mode at a time. We performed two-photon polarization state tomography [44] both before and after up-conversion using an overcomplete set of 36 projective measurements, corresponding to the polarization states $|H\rangle$, $|V\rangle$, $|\pm\rangle = (1/\sqrt{2})(|H\rangle \pm |V\rangle)$, and $|\pm i\rangle = (1/\sqrt{2})(|H\rangle \pm i|V\rangle)$. Because of the polarization-dependent diffraction efficiency of our grating, we performed projective polarization measurements before diffraction. A removable mirror was used to couple the single-photon signal into D_{in} to characterize the input state, which was found to have an average fidelity [45] of 96.2% with $|\Phi^+\rangle$ over the three potential modes and an average tangle [46] of 0.88. The up-converted states were reconstructed without background subtraction and found to have fidelities $(88.6 \pm 0.3)\%$, $(95.1 \pm 0.3)\%$, and $(92.9 \pm 0.4)\%$ with $|\Phi^+\rangle$ and tangles of 0.737 ± 0.020, 0.828 ± 0.011, and 0.836 ± 0.015, for modes A–C, respectively, where the error bars are determined by Monte Carlo simulation assuming Poissonian counting statistics. These two figures of merit explicitly demonstrate that quantum correlations are maintained through the bandwidth compression process.

We next prepared the pump to produce down-converted states in modes A and B. We studied the case (i) where the pump was set to produce the separable states $|VV\rangle$ and

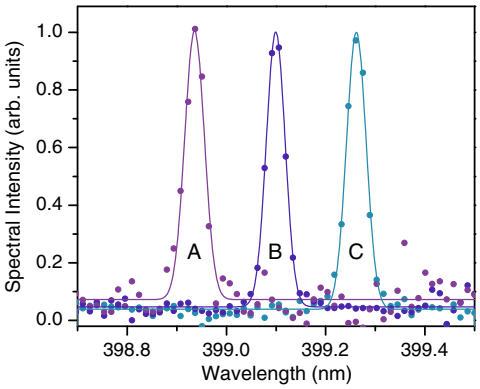

FIG. 2 (color online). Up-converted single-photon spectra for each temporal mode. We prepared the pump to maximize the count rate in each of the three temporal modes and measured the spectra shown (with background subtraction). The time delay between the modes maps each to a distinct central wavelength and the spectral bandwidth is compressed by a factor of 20 relative to the input.

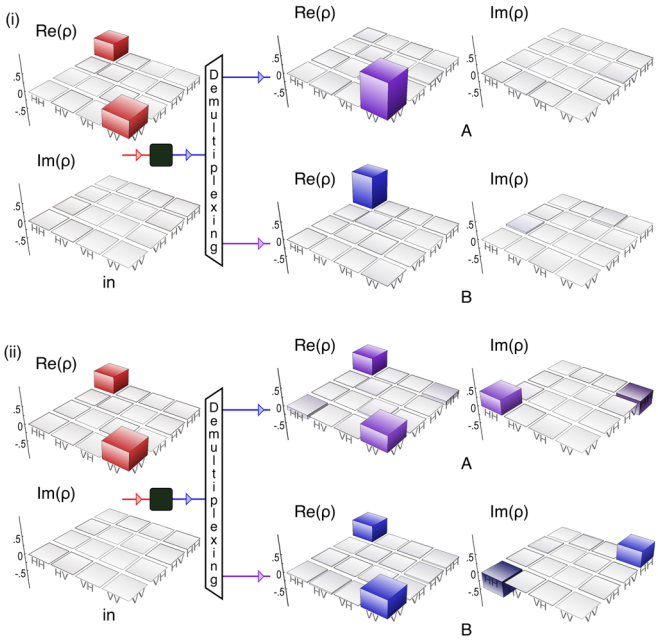

FIG. 3 (color online). Demultiplexing two orthogonal states. With the pump prepared in modes A and B to either produce (i) orthogonal separable states or (ii) orthogonal maximally entangled states, the density matrices measured before time-to-frequency conversion (left) appear the same, with negligible coherences. After demultiplexing, the experimentally reconstructed output density matrices (right) are revealed to describe vastly different quantum states, which are separable in case (i) but show a high degree of entanglement in case (ii).

$|HH\rangle$ [Fig. 3(i)], and the case (ii) where the pump was set to produce the maximally entangled states $|\Phi^{+i}\rangle = (1/\sqrt{2})(|HH\rangle + i|VV\rangle)$ and $|\Phi^{-i}\rangle = (1/\sqrt{2})(|HH\rangle - i|VV\rangle)$ [Fig. 3(ii)], in modes A and B, respectively. The reconstruction from the coincidence measurements between D_{in} and D_{idler} produced the density matrix on the left-hand side of Fig. 3, with large populations in $|HH\rangle$ and $|VV\rangle$ but negligible coherence; both reconstructions have fidelities of 98% with an equal mixture of $|HH\rangle$ and $|VV\rangle$. This arises because the detector is not fast enough to resolve the pulses, instead measuring a mixture of the two signals and obfuscating the underlying quantum coherences of the individual states. By measuring the photons after the up-conversion setup, the density matrices shown on the right side of Fig. 3 were reconstructed. The density matrices in case (ii) exhibit large quantum coherences, which are required for entanglement, while those for case (i) do not, as expected for separable states. Indeed, the density matrices reconstructed in case (i) have an average fidelity of $(93.6 \pm 0.3\%)$ with the target separable states, and those in case (ii) have an average fidelity of $(91.2 \pm 0.5\%)$ with the expected maximally entangled states and an average tangle of 0.714 ± 0.014.

We then prepared the pump to produce maximally entangled states into all three modes, using the pump polarization sequence $|-i\rangle$, $|+\rangle$, and $|+i\rangle$ for modes A–C. We measured the states initially and after the up-conversion process, shown in (Fig. 4). The initial state has fidelity 97.6% with the nonmaximally entangled mixed state resulting from an incoherent mixture of the three expected maximally entangled states in modes A–C with weighting 0.25, 0.5, and 0.25, determined by the ratios of the intensities of the three pump pulses. The output states each exhibit different quantum correlations yet are all highly entangled, with fidelities of $(77.3 \pm 0.9)\%$, $(91.5 \pm 0.4)\%$, and $(86.1 \pm 0.7)\%$ with the expected maximally entangled states and tangles of (0.40 ± 0.2), (0.720 ± 0.013), and (0.58 ± 0.02) for modes A–C, respectively. The coincidence rates for modes A and C were half that of mode B due to the distribution of pump power, and their reconstructed states were thus more affected by background noise; however, cross talk between signals was not a significant issue in our experiment. Additional experimental results for different pump preparations may be found in the Supplemental Material [38].

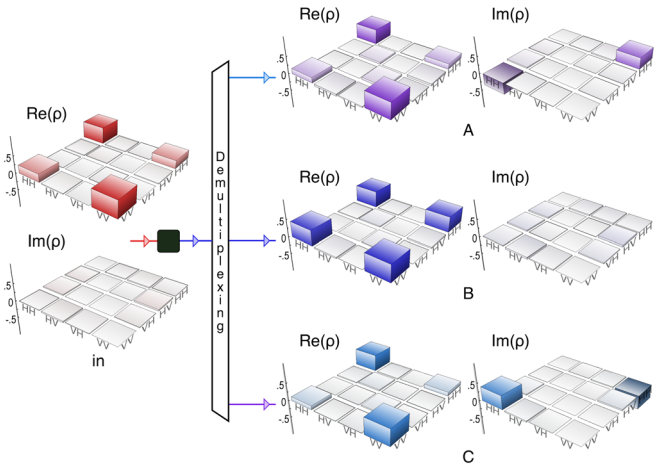

FIG. 4 (color online). Demultiplexing three entangled states. The pump was prepared to produce a train of three maximally entangled states. Weak coherences are seen in the density matrix measured before time-to-frequency conversion (left), with a calculated tangle of 0.21. After being demultiplexed, all three experimentally reconstructed density matrices show much stronger coherence and larger entanglement, with tangles of 0.40, 0.72, and 0.58 in modes A–C, respectively.

We have demonstrated the conversion of a train of up to three temporally spaced single-photon pulses to a comb of distinct frequencies while maintaining quantum correlations in polarization. We have shown that this method can distinguish picosecond-separated single photons using detectors with nanosecond-scale time resolution. Improvements to the efficiency may be possible through the use of periodically poled nonlinear materials [20,21] and cavity enhancements [47]. With higher conversion efficiencies, this ultrafast readout of time-division-multiplexed entangled quantum signals could be used to increase the density of quantum information carried through a single physical medium or to distribute quantum states throughout a multiuser network by applying time-to-frequency conversion to both signal and idler photons. Our results also demonstrate tunable bandwidth compression of a polarization-entangled photon [32,48,49]. More generally, our work demonstrates how shaped laser pulses may be used to manipulate the spatiotemporal waveforms of single photons while preserving quantum information.

The authors thank M. D. Mazurek, A. Martin, K. A. G. Fisher, and M. Agnew for helpful discussions. We are grateful for financial support from NSERC, CFI, OCE, Industry Canada, the Canada Research Chairs Program, and the Ontario Ministry of Research and Innovation.

*jdonohue@uwaterloo.ca

[1] C. H. Bennett and G. Brassard, in *Proceedings of IEEE International Conference on Computers, Systems and Signal Processing, New York, 1984* (IEEE, New York, NY, 1984), Vol. 175.
[2] C. H. Bennett, G. Brassard, C. Crépeau, R. Jozsa, A. Peres, and W. K. Wootters, Phys. Rev. Lett. **70**, 1895 (1993).
[3] A. K. Ekert, Phys. Rev. Lett. **67**, 661 (1991).
[4] A. Acin, N. Gisin, and L. Masanes, Phys. Rev. Lett. **97**, 120405 (2006).
[5] C. A. Brackett, IEEE J. Sel. Area Comm. **8**, 948 (1990).
[6] S. Kawanishi, IEEE J. Quant. Electron. **34**, 2064 (1998).
[7] P. D. Townsend, Electron. Lett. **33**, 188 (1997).
[8] G. Brassard, F. Bussieres, N. Godbout, and S. Lacroix, in *Applications of Photonic Technology* (SPIE, Bellingham, WA, 2003), pp. 149–153.

[9] J. Chen, G. Wu, L. Xu, X. Gu, E. Wu, and H. Zeng, New J. Phys. **11**, 065004 (2009).
[10] B. Qi, W. Zhu, L. Qian, and H.-K. Lo, New J. Phys. **12**, 103042 (2010).
[11] I. Choi, R. J. Young, and P. D. Townsend, Opt. Express **18**, 9600 (2010).
[12] M. Sasaki, M. Fujiwara, H. Ishizuka, W. Klaus, K. Wakui, M. Takeoka, S. Miki, T. Yamashita, Z. Wang, A. Tanaka *et al.*, Opt. Express **19**, 10 387 (2011).
[13] I. Herbauts, B. Blauensteiner, A. Poppe, T. Jennewein, and H. Huebel, Opt. Express **21**, 29 013 (2013).
[14] R. Hadfield, Nat. Photonics **3**, 696 (2009).
[15] C. Bennett and B. Kolner, Opt. Lett. **24**, 783 (1999).
[16] I. A. Walmsley and C. Dorrer, Adv. Opt. Photonics **1**, 308 (2009).
[17] M. A. Foster, R. Salem, Y. Okawachi, A. C. Turner-Foster, M. Lipson, and A. L. Gaeta, Nat. Photonics **3**, 581 (2009).
[18] D. Shayovitz, H. Herrmann, W. Sohler, R. Ricken, C. Silberhorn, and D. M. Marom, Opt. Express **20**, 27 388 (2012).
[19] Y.-H. Kim, S. P. Kulik, and Y. Shih, Phys. Rev. Lett. **86**, 1370 (2001).
[20] A. P. Vandevender and P. G. Kwiat, J. Mod. Opt. **51**, 1433 (2004).
[21] C. Langrock, E. Diamanti, R. V. Roussev, Y. Yamamoto, M. M. Fejer, and H. Takesue, Opt. Lett. **30**, 1725 (2005).
[22] S. Tanzilli, W. Tittel, M. Halder, O. Alibart, P. Baldi, N. Gisin, and H. Zbinden, Nature (London) **437**, 116 (2005).
[23] S. Ramelow, A. Fedrizzi, A. Poppe, N. K. Langford, and A. Zeilinger, Phys. Rev. A **85**, 013845 (2012).
[24] A. P. VanDevender and P. G. Kwiat, Opt. Express **15**, 4677 (2007).
[25] M. A. Hall, J. B. Altepeter, and P. Kumar, Phys. Rev. Lett. **106**, 053901 (2011).
[26] A. Pe'er, B. Dayan, A. A. Friesem, and Y. Silberberg, Phys. Rev. Lett. **94**, 073601 (2005).
[27] S. E. Harris, Phys. Rev. Lett. **98**, 063602 (2007).
[28] K. A. O'Donnell and A. B. U'Ren, Phys. Rev. Lett. **103**, 123602 (2009).
[29] D. Kielpinski, J. F. Corney, and H. M. Wiseman, Phys. Rev. Lett. **106**, 130501 (2011).
[30] A. Eckstein, B. Brecht, and C. Silberhorn, Opt. Express **19**, 13 770 (2011).
[31] M. T. Rakher, L. Ma, M. Davanço, O. Slattery, X. Tang, and K. Srinivasan, Phys. Rev. Lett. **107**, 083602 (2011).
[32] J. Lavoie, J. M. Donohue, L. G. Wright, A. Fedrizzi, and K. J. Resch, Nat. Photonics **7**, 363 (2013).
[33] J. M. Lukens, A. Dezfooliyan, C. Langrock, M. M. Fejer, D. E. Leaird, and A. M. Weiner, Phys. Rev. Lett. **112**, 133602 (2014).
[34] J. M. Donohue, M. Agnew, J. Lavoie, and K. J. Resch, Phys. Rev. Lett. **111**, 153602 (2013).
[35] F. Raoult, A. C. L. Boscheron, D. Husson, C. Sauteret, A. Modena, V. Malka, F. Dorchies, and A. Migus, Opt. Lett. **23**, 1117 (1998).
[36] K. Osvay and I. N. Ross, Opt. Commun. **166**, 113 (1999).
[37] R. Kaltenbaek, J. Lavoie, D. N. Biggerstaff, and K. J. Resch, Nat. Phys. **4**, 864 (2008).
[38] See Supplemental Material at http://link.aps.org/supplemental/10.1103/PhysRevLett.113.163602 for a theoretical examination of the up-conversion demultiplexing effect and additional details on experimental methods.
[39] P. G. Kwiat, E. Waks, A. G. White, I. Appelbaum, and P. H. Eberhard, Phys. Rev. A **60**, R773 (1999).
[40] Y.-H. Kim, S. P. Kulik, and Y. Shih, Phys. Rev. A **62**, 011802 (2000).
[41] B. Dromey, M. Zepf, M. Landreman, K. O'Keeffe, T. Robinson, and S. Hooker, Appl. Opt. **46**, 5142 (2007).
[42] E. Treacy, IEEE J. Quantum Electron. **5**, 454 (1969).
[43] ITU Recommendation, G.694.1 Spectral grids for WDM applications: DWDM frequency grid (2012).
[44] D. F. V. James, P. G. Kwiat, W. J. Munro, and A. G. White, Phys. Rev. A **64**, 052312 (2001).
[45] R. Jozsa, J. Mod. Opt. **41**, 2315 (1994). The fidelity between density matrices $\boldsymbol{\rho}$ and $\boldsymbol{\sigma}$ is $\mathbf{Tr}[\sqrt{\sqrt{\boldsymbol{\sigma}}\boldsymbol{\rho}\sqrt{\boldsymbol{\sigma}}}]^2$.
[46] V. Coffman, J. Kundu, and W. K. Wootters, Phys. Rev. A **61**, 052306 (2000). The tangle is the square of the concurrence.
[47] S. Sensarn, I. Ali-Khan, G. Y. Yin, and S. E. Harris, Phys. Rev. Lett. **102**, 053602 (2009).
[48] W. P. Grice and I. A. Walmsley, Phys. Rev. A **56**, 1627 (1997).
[49] J. Lavoie, R. Kaltenbaek, and K. J. Resch, New J. Phys. **11**, 073051 (2009).